International Communications in Heat and Mass Transfer 142 (2023) 106658

Contents lists available at ScienceDirect

International Communications in Heat and Mass Transfer

journal homepage: www.elsevier.com/locate/ichmt

Experimental investigation of variable fin length on melting performance in a rectangular enclosure containing phase change material

Umit Nazli Temel *, Ferhat Kilinc

Department of Mechanical Engineering, Sivas Cumhuriyet University, 58140 Sivas, Turkey

ARTICLE INFO

Keywords:
Phase change material
Latent heat storage
Variable fin length
Melting
Infrared thermography

ABSTRACT

The present study proposes a new technique to determine liquid fractions of phase change material during the melting process in a left-side heated rectangular enclosure. The effects of variable fin length arrangements on the melting performance of phase change material (PCM) were also investigated experimentally. Detailed information about solid, mushy, and liquid ratios was obtained by analysing the temperature histograms of real thermal images of the melting zone. In accordance with the nature of the melting, the use of variable-length fins shortens the melting time by 14.9% compared to the equal-length fin arrangement. Similarly, variable-length fins reduce the average temperature of the latent heat thermal energy storage (LHTES) by around 10 °C compared to the equal-length fin arrangement. The use of variable length fin arrangements ensures a more homogeneous melting process within the LHTES. The fin arrangement evenly distributed to the entire heating source is more effective at low heating rates. In contrast, fin arrangements evenly distributed over the lower half of the heating source are more efficient at high heating rates.

1. Introduction

The intermittent nature of renewable energy sources, the discrepancy between the energy supply and demand, and the recovery of the waste heat from the thermal systems increase energy storage's importance from today to the future. Phase change material (PCM) based latent heat thermal energy storage (LHTES) is the promising method due to its high energy density and widespread potential usage. In this method, energy is stored within the PCM by a phase change process and is released by the reverse process for later use. Solid-liquid PCMs are preferred more, due to the small volume change during phase change [1]. LHTES systems based on solid-liquid PCM have been used in numerous applications depending on the melting temperature for providing the energy savings such as domestic refrigerators [2], passive heating and cooling of buildings [3,4], air conditioning systems [5], solar energy conversion systems [6,7] and waste heat recovery systems [8,9]. Another application area of the LHTES systems is the thermal protection of some devices, such as battery packs, electronic devices [10] and the transportation of blood and organs [11,12] to maintain their biological activities. However, the major disadvantages of PCMs are their low thermal conductivity, which directly affects the energy charge/discharge rate and efficient storage.

In order to use LHTES systems effectively, some techniques have been developed on PCM to enhance the heat transfer mechanism. The use of metal foams [13,14] has problems such as leakage and limitation of the amount of PCM absorbed into the pores. The dispersion of metal and carbon-based nanoparticles [15,16] have been widely used to enhance PCM thermal conductivity. Although the decrease in latent heat is acceptable, the increase in dynamic viscosity adversely affects the heat transfer mechanism in the liquid phase because it prevents buoyancy-driven flow movements.

However, adding fins into the PCM to improve the heat transfer of the LHTES is widely preferred as it is an easy, economical and effective method. Hosseinizadeh et al. [17] carried out an experimental and numerical investigation of a PCM-based LHTES in a rectangular container equipped with vertical fins. They reported that increasing the number of fins and fins length increases the thermal performance of LHTES, whereas increasing the fin thickness has no significant effect. Abdi et al. [18] conducted a parametric study numerically to enhance the charge rate by varying the fin length and the number of fins in a cavity with vertically oriented fins. They reported that using longer fins offers a higher rate of heat transfer rather than increasing the number of fins. Acır et al. [19] evaluated the melting performance of PCM experimentally, in a container equipped with vertical fins in terms of fin number (*n*

* Corresponding author.
E-mail address: untemel@cumhuriyet.edu.tr (U.N. Temel).

https://doi.org/10.1016/j.icheatmasstransfer.2023.106658

Available online 11 February 2023

= 3, 5, 7) and thickness (t = 1 mm, 1.5 mm, 2 mm). They realized that the melting performance of the top-heated container increased with the number of fins, whereas it decreased with fin thickness. Similarly, Huang et al. [20] realized that increasing the number of fins within the rectangular LHTES reduced the melting time and made the temperature distribution more uniform. Although fins enhance the energy storage rate, they lead to an increase in system weight and a decrease in the amount of PCM (or energy storage capacity) of the LHTES. Actually, the dominated heat transfer mechanism starts to change from conduction to natural convection with the onset of PCM melting [21]. However, increasing the number of fins causes conduction to remain the dominant heat transfer mechanism even in the liquid state. In fact, natural convection driven by the buoyancy force is an important advantage that should not deteriorate in terms of increasing the storage rate of energy in LHTES systems. This requires the number of fins in the container should be limited to use the beneficial effects of natural convection.

In some cases, space constraints and other reasons necessitated the use of side-heated LHTES systems equipped with horizontal fins. Kamkari and Shokouhmand [22] conducted an experimental investigation to visualize the transient melting phenomena of the side-heated rectangular enclosures with and without horizontal fins. They reported that there is an optimum value for the number of fins to be placed in LHTES and increasing the number of fins from 0 to 3 reduces the melting time. Tian et al. [23] conducted a detailed numerical study to investigate the fin material effect on LHTES performance in a side-heated rectangular LHTES. They compared the effects of aluminium, copper, carbon steel and steel 302 fins to improve LHTES performance in terms of criteria such as surface averaged Nusselt number, melting time, total stored energy, mean power, stored energy per mass and cost per energy stored. They stated that the most suitable fin material in terms of the mentioned criteria is aluminium. When considering the melting history of the PCM in the vertical side-heated LHTES, it is clear that the positioning of the horizontal fins will be effective. For instance, it is determined that varying fin spacing has a marginal impact on heat storage performance [24]. Ji et al. [25] numerically investigated the effects of fins angle on the melting performance of vertical-side heated LHTES. They found that fins at the downward angle of 15^{o} accelerate the PCM melting better than other orientations. In another study, Ji et al. [26] numerically investigated the effects of varying fin lengths on LHTES performance for double fin arrangements. They revealed that in the premise of constant total fins length, the arrangement of a short upper fin and long lower fin can positively enhance the PCM melting rate.

Some researchers have investigated the melting-solidification process of PCMs by using infrared (IR) technologies. Zhang et al. [27] investigated the role of the partial and gradient filling strategies of copper foam on the performance of LHTES. The movement of the melting front of the copper foam/paraffin composite at different filling ratios and the change in the temperature field were visualized with a thermal camera. They reported that the PCM melting rate increased first and then decreased with an increasing filling ratio, reaching its maximum value when the filling ratio was 5/6. Korti et al. [28] analysed the effects of LHTES inclination by visualizing the solid-liquid interface with an infrared camera. They reported that the inclination angle strongly affects the melting front progression, and the total melting time of the inclined cavity is 48% shorter than that of the vertical cavity. Fadl et al. [29] experimentally investigated the effect of different heat flux intensities on the melting performance of PCM in a rectangular test cell. They used an imaging technique to visualize the movement of the solid-liquid interface by using the camera. Their results indicate that there is a strong correlation between wall heat flux and convective flow. Okabe et al. [30] developed an infrared thermography technique to characterize natural convection heat flow while melting PCM in a rectangular enclosure heated from below. They determined the spatio-temporal variation of the heat transfer coefficient at different heat flux and inclination angles. They found that the heat transfer mechanism changes continuously based on melting stages, and that heat flux and inclination angle greatly affect it. In these studies, the focus was on obtaining temperature contours related to the melting of PCM. In some studies, experimental liquid-solid fractions were obtained using image processing techniques on the solid-liquid interface captured with a digital camera.

Nowadays, determining appropriate horizontal fin positions and arrangements based on the nature of the melting in vertical side-heated LHTES systems is still a challenge for performance improvements. Most studies on this subject have focused on numerical studies, and there is a lack of experimental cases. Therefore, the present experimental study aims to enhance the overall PCM melting by using triple fins arrangement with variable length in a vertical side-heated LHTES. In this respect, the effects of upwardly decreasing triple fins arrangements on the melting performances were experimentally measured. The findings were compared with the equal length triple fins arrangement and the finless condition. The effects of applying the triple fins arrangement to the lower half side of the LHTES were also examined. Performance evaluations were carried out in terms of total melting time and uniform temperature distribution for all cases. Another novelty of the study was the proposal of a new technique for determining liquid fractions of the melting process experimentally. For this purpose, time-dependent melting visualization was obtained experimentally for all cases. The determination of liquid fractions from the obtained thermal visualization was determined experimentally using a new method based on temperature distribution for the first time in the literature.

2. Material and methods

The thermal storage material used in this study was a paraffin-based PCM called A42 available from PlusICE (UK). Temperature-dependent thermal conductivity measurements of A42 were conducted with the KD2 Pro device (Decagon Devices Inc., USA) at different temperatures for solid and liquid phases. This device works based on the transient linear heat source principle over a certain time. The sensors of the KD2 Pro operate as both a heater and a temperature sensor during the heating period. The thermal conductivity values are determined by analysing the measured temperatures over time. Solid state measurements were obtained from the sample produced using the mould in Fig. 1 using the relevant sensor (TR1) of the device. The mould is an acrylic tube with a diameter of 30 mm and a height of 120 mm and is equipped with a shaft to leave a 100 mm height and 2.4 mm diameter gap on the sample axis to allow the sensor entry. The solid sample was prepared by pouring molten liquid PCM into a mould and solidifying at room temperature. Similar steps were performed for the liquid phase measurements. An axially immersed sensor (KS2) to the liquid PCM within a cylindrical glass container with a 20 mm diameter was used to measure liquid states. The accuracy of the device in the 0.2–2 W/mK range is 10% for solids and 5% for liquids. At least five measurements were made for each sample, and average values were recorded with a standard deviation of 0.5%. The thermal conductivity measurements at different temperatures were carried out by using an air conditioner cabinet. All thermal conductivity measurements were performed after thermal equilibrium was achieved at the relevant temperature in the air-conditioning cabinet.

The calorimetric properties of A42 were measured by using Differential Scanning Calorimetry (DSC-60 Shimadzu, Japan). Approximately 5 mg of A42 particles were confined in a special DSC container, and a measurement sample was prepared. The DSC was adjusted to scan the temperature range from 20 °C to 60 °C with an increment rate of 2 °C/min. The calorimetric sensitivity and temperature accuracy of the DSC device is ±1% and ± 0.1 °C. At least three measurements were made, and average values were recorded with a standard deviation of 1%.

In the present study, experimental procedures were carried out using the test setup shown in Fig. 2. The experimental setup consists of a thermal camera, DC power supply, computer, thermocouples, data logger, and LHTES. The LHTES is made from plexiglass material of 5 mm thickness in accordance with thermal and real-time image capture. The

Fig. 1. The stages of measuring solid phase thermal conductivity.

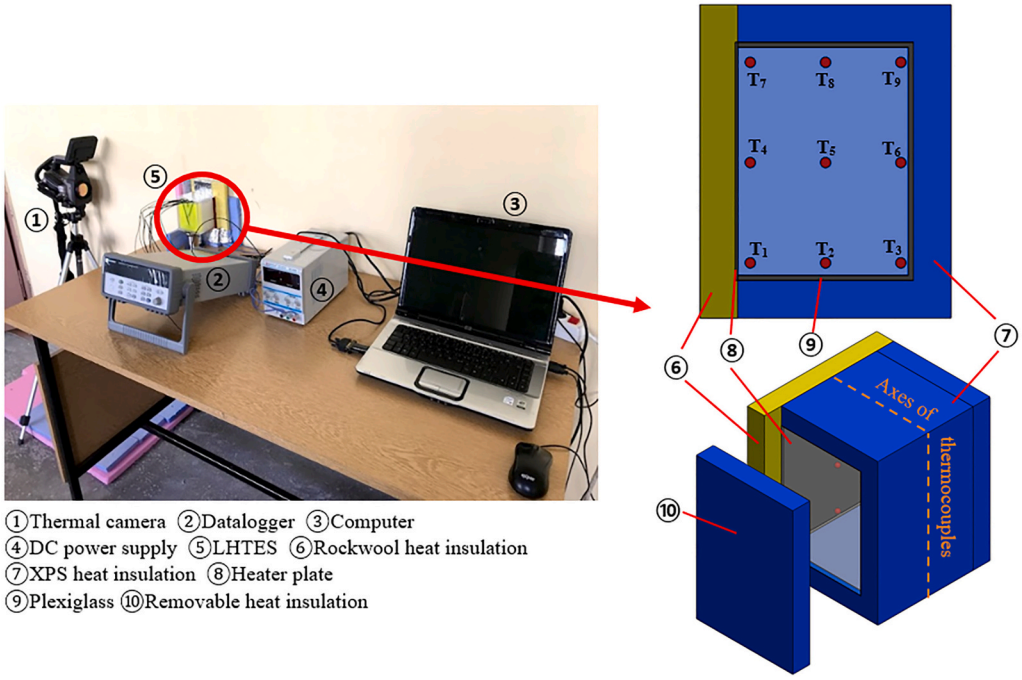

Fig. 2. The experimental setup used for thermal performance tests.

LHTES container with dimensions of 100 mm × 90 mm × 75 mm was obtained by bonding carefully cut plexiglass plates with chloroform (CHCl3). Only the left wall of LHTES was replaced with a 1 mm thick 100 mm × 90 mm aluminium plate. The fin arrangements shown in Fig. 3 were tightly fitted to the aluminium plate. In the Fin 1 arrangement, three fins of equal length (50 mm) are equally spaced on the left wall of the LHTES. In the Fin 2 arrangement, upwardly shortened three fins (65 mm–50 mm-35 mm) are equally spaced on the left wall of the LHTES. The Fin 3 arrangement is the application of the Fin 2 arrangement to the lower half side of the LHTES. Additionally, another LHTES without fins was created for comparison of performance (Finless case). The LHTES configurations were prepared by liquefying A42 on a hot-plate, pouring into the LHTES container, and solidifying it for 24 h at room temperature. A 100 mm × 100 mm plate heater is mounted on the left side aluminium plate of all LHTES models from the outside as shown in Fig. 2. All LHTES models are thermally insulated to minimize the amount of heat lost to the outside. On the back side of the heater, 30 mm rock wool was used as insulation material due to its high-temperature resistance. Similarly, the plexiglass walls are covered with a 50 mm extruded polystyrene foam (XPS) board due to its easy applicability. A removable insulation plate was applied to the wall on one side, allowing thermal camera image acquisition. As can be seen in Fig. 2, time-dependent temperature measurements were taken at nine different points along the vertical symmetry plane of the LHTES. This choice is reasonable since the LHTES walls are completely insulated, causing melting to occur in two dimensions. The K-type thermocouples with an accuracy of ±0.5 °C have gathered temperature data at 30 s intervals through a data collector (Agilent 34970A) and transferred it to a computer.

Thermal images were captured using a thermal camera with a sensitivity of 0.08 °C (ThermaCam S65, FLIR Systems, Sweden). It works by measuring and imaging the infrared radiation emitted by objects. The change of colour palettes, emissivity settings, or temperature range change can be adjusted as desired. The infrared radiation emitted from an object is a function of the object's temperature. The thermal camera gives the temperature contour of objects by measuring the radiation. Metallic surfaces have a negative effect on infrared images due to the glare effect. To avoid this difficulty, the camera is positioned in a way

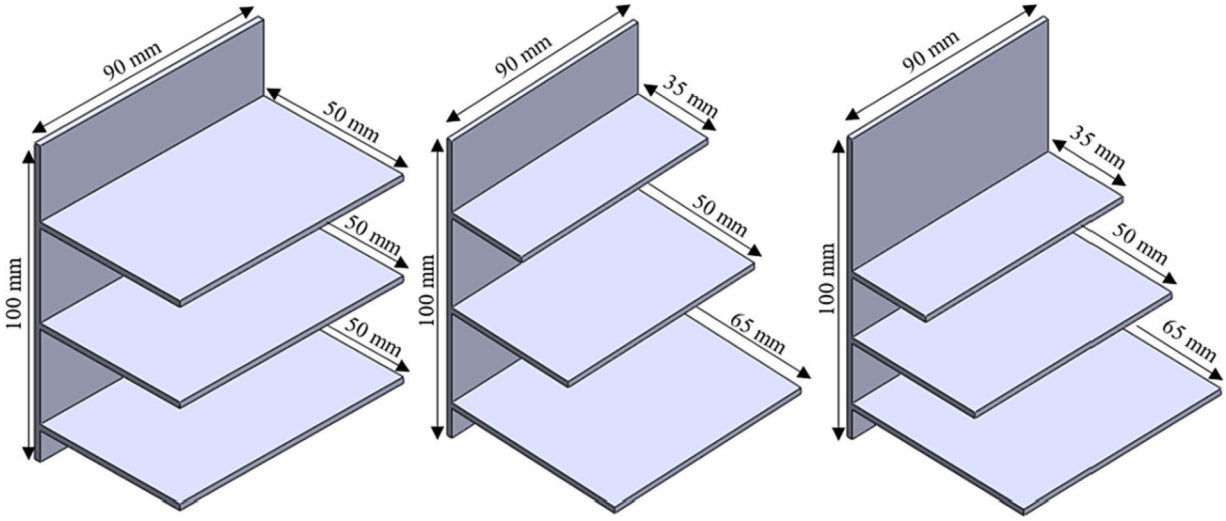

Fig. 3. Different fin arrangements used within the LHTES (Fin1, Fin2 and Fin3, left to right).

that the angle between the direction of view and the normal of the metallic heater is 90°. During image acquisition, the removable insulation plate on the camera-facing wall of the LHTES was removed for a very short duration and then reattached.

The ThermaCAM Researcher software was used to create temperature contours from thermal camera infrared (IR) images. It is also possible to analyse temperature contours in detail with the ThermaCAM Researcher. However, the temperature contour obtained from the thermal camera needs to be calibrated according to the thermocouple values since it is a function of the radiation emitted by the outer LHTES wall. Korti et al. [28] also adopted a similar method, the use of temperature measurement with thermocouples to adjust the infrared measurements. Following are the steps that were followed during calibration; i) the average temperature was determined for the PCM using temperature measurement data through nine different thermocouples for the desired time instant, ii) The average temperature of the infrared temperature contour taken from the LHTES outer wall was determined by the ThermaCAM Researcher program, iii) the calibration of the temperature contour taken from the LHTES outer wall to the inner PCM temperature contour was performed by adjusting the emissivity value. The ThermaCAM Researcher program calculated the emissivity value as a coefficient that makes the LHTES outer wall average temperature equal to the PCM average temperature. The emissivity values used are between 0.60 and 0.85. It increases as the LHTES outer wall temperature rises and the temperature difference between the PCM and the LHTES outer wall increases.

Uncertainty analysis is important in terms of the precision of the measured results and the accuracy of the results obtained. To obtain the uncertainty values, the following equation was used [31],

$$w_R = \left[\left(\frac{\partial R}{\partial x_1} w_1\right)^2 + \left(\frac{\partial R}{\partial x_2} w_2\right)^2 + \ldots + \left(\frac{\partial R}{\partial x_n} w_n\right)^2\right]^{1/2} \quad (1)$$

where R is a function of independent variables ($x_{1,2,n}$) and resulting from the experimental study. $w_{R,1,2,n}$ can be taken as the uncertainties in the independent variables. According to the uncertainty analysis, the values estimated as ±2% for the reading accuracy of the thermal camera, ±0.5% for K- type thermocouples, ±6% for DC power supply, and ± 0.4% for thermocouple measurement accuracy of the data acquisition system (datalogger). The total uncertainty value is estimated as ±6.53% for the whole system.

3. Results and discussions

The thermal conductivity values at certain temperatures that A42 organic PCM was exposed to the melting process are given in Fig. 4. The thermal conductivity of solid A42 at room temperature was measured as 0.22 W/mK at T = 20 °C and this value is insufficient in terms of effective energy storage rate in LHTES systems. Moreover, with the transition to the liquid phase, the thermal conductivity decreases (at $T >$ 40 °C k = 0.15 W/mK) further due to molecular disorder. These results support the necessity of thermal enhancement of PCM in energy storage processes.

The melting phase thermal properties of the A42 were obtained by analysis of the DSC endotherm curve given in Fig. 5. Although the organic PCM used in the study is called A42, it performs the melting onset (T_{om} = 32.2 °C) and endset (T_{em} = 41 °C) processes in a relatively wide temperature range due to the low thermal conductivity. The area of the region between the DSC peak and the baseline is the latent heat of melting, and it was measured as H_e = 109.7 J/g as a result of the analysis.

The instantaneous thermal camera images (IR and SD) for different fin arrangements and finless case were shown in Fig. 6 with 10 min intervals between 20 and 60 min. It should be noted that IR images of the thermal camera are essentially temperature contours obtained experimentally. If the scale of the temperature contours is adjusted between

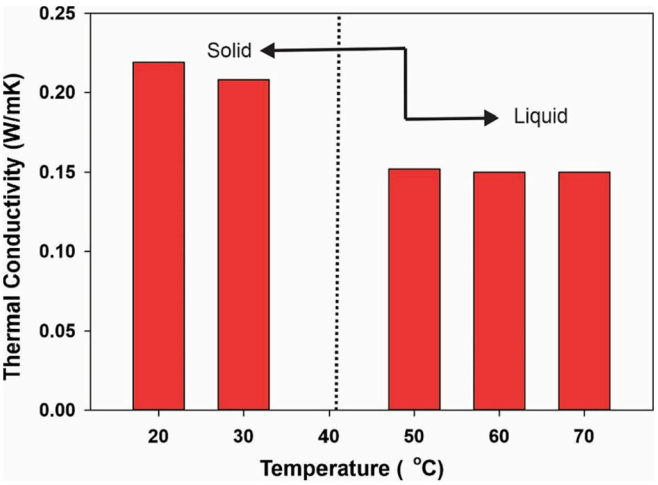

Fig. 4. Thermal conductivity values at different temperatures.

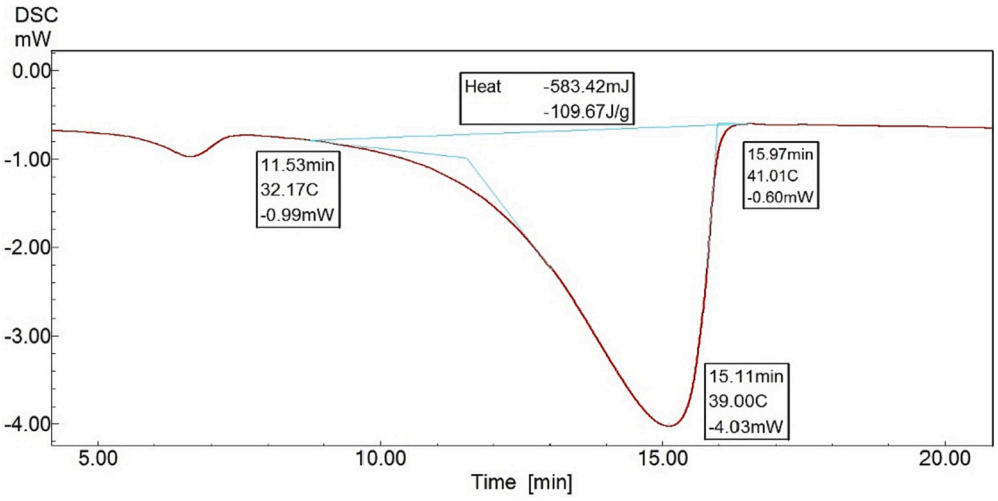

Fig. 5. DSC analysis for PCM.

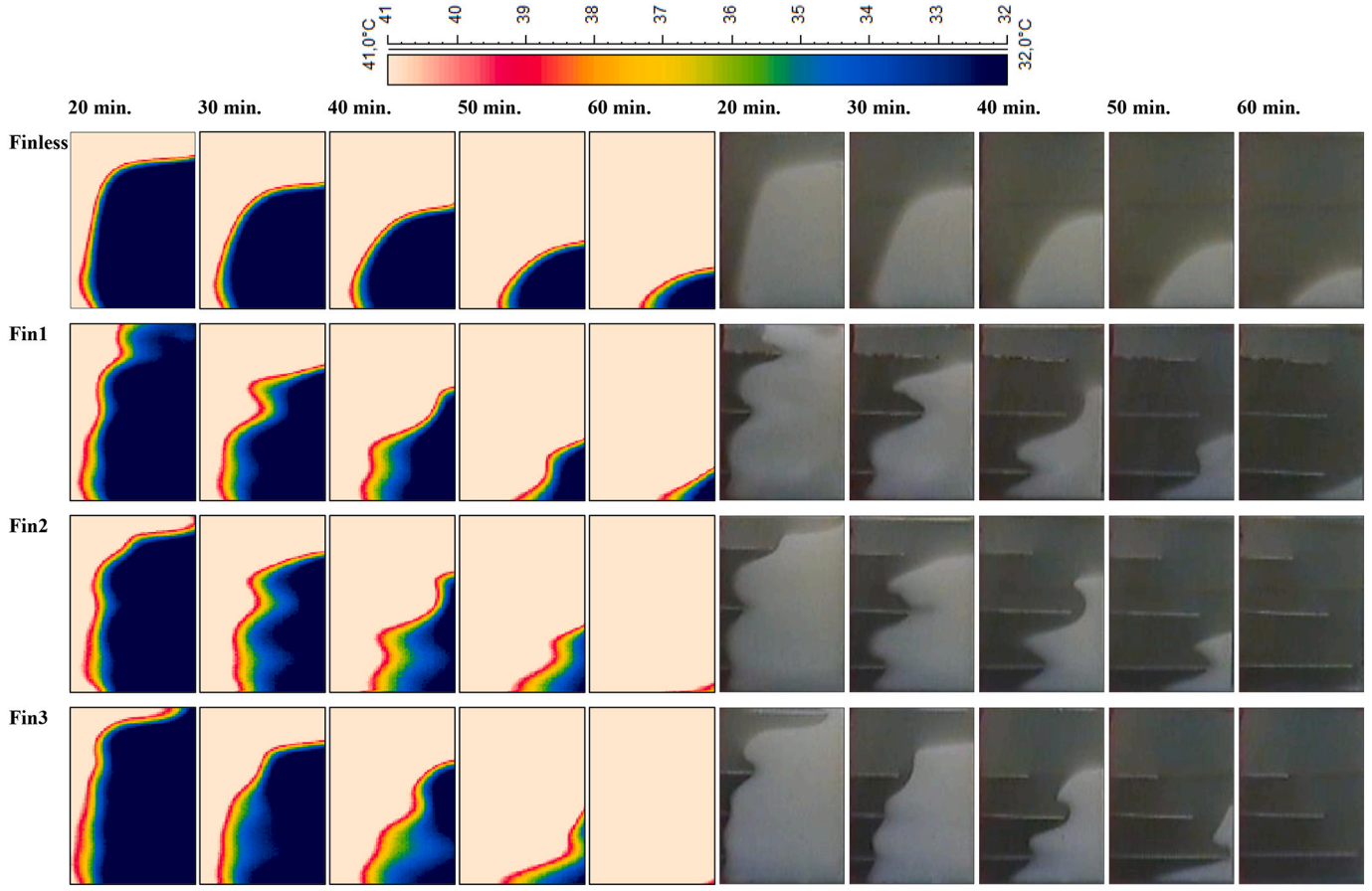

Fig. 6. Time-dependent thermal (IR) and real images (SD) of LHTES with finless and different types of fins at 50 W.

onset melting and endset melting temperatures, resulted images correspond to the liquid fractions according to the below eqs.

$$LF = 0 \text{ if } \left(T < T_{om} = 32^{o}C\right) LF = 1 \text{ if } \left(T > T_{em} = 41^{o}C\right) LF = \frac{T - T_{om}}{T_{em} - T_{om}} \text{ if } \left(T_{om} < T < T_{em}\right) \quad (2)$$

where T is the PCM temperature, and $T_{om} = 32\ ^{\circ}C$ and $T_{em} = 41\ ^{\circ}C$ are the melting onset and melting endset temperatures obtained from DSC analyses. Accordingly, in thermal camera images, the cream-colored region is liquid, the dark blue region is solid, and the colored region between them is the transition region called the mushy zone.

Initially thin and uniform liquid PCM layer occurs along the height of the left-side heated LHTES with the finless case, under the effect of the conduction heat transfer mechanism. When the fluid reaches a sufficient thickness, the buoyancy-driven flow mechanism becomes dominant, and the liquid PCM rises along the heater wall and descends along the solid-liquid interface, creating a clockwise circulating current. In this case, the hot upper region and the cold lower region are formed within

the LHTES. As seen in Fig. 4, the sharp decrease in thermal conductivity in the liquid phase indicates that melting occurs predominantly under the influence of buoyancy currents. In other words, the downward movement of the hot PCM in the upper region of the LHTES along the solid-liquid interface is the primary cause of the melting. However, the melting rate slows in the lower right corner of the LHTES due to the cooling of the hot PCM during its downward movement. Therefore, for the LHTES heated from the left side, the region that will naturally melt last is the lower left corner.

This result suggests that if the melting performance of LHTES is improved by adding fins, placement should be appropriate for the nature of the melting. For this reason in the current study, LHTES was equipped with triple fin structures that had equal total surface areas as follows, i) Evenly spaced and of equal length throughout the heater (Fin 1), for comparison purposes, ii) Appropriate to the nature of the melting, upwardly shortened and evenly spaced throughout the heater (Fin 2), iii) Evenly spaced placement of the Fin 2 arrangement in the lower half of the heater (Fin 3).

All of the fin arrangements exhibit worse melting performance than the finless case during the first 30 min. The cause is that the circulating currents formed in the left and upper corners of the LHTES are blocked by the fins. On the other hand, fin arrangements accelerate the formation of the mushy zone with the heat transferred to the PCM inner region along the fin from left to right. Additionally, due to the shorter middle and upper fins compared to the Fin 1 arrangement, the buoyancy-driven flows trapped between the parallel fins in Fin 2 and Fin 3 arrangements are released after 40 min. The melting performance of the Fin 2 and Fin 3 arrangements improves, with the fast transition of PCM to liquid in the mushy region and the formation of circulating flow that dominates the whole LHTES. Fin arrangements appropriate for the nature of the melting (Fin 2 and Fin 3) are more successful than Fin 1 in melting the critical right lower region. It is clear that the extension of the fin length, which is shortened from the upper region because it is not needed, to the critical lower region is effective in that. The calculation of the liquid fractions obtained visually in Fig. 7 was determined experimentally using a new method for the first time in the literature. Similar studies in the literature employed image processing techniques to determine liquid fractions from digital images taken with a camera. In this technique, a distinction is made by making use of the colour difference of liquid and solid PCM. On the other hand, in the current study, the liquid fraction of the PCM was calculated using the temperature histograms created by analysing the infrared temperature contours.

Moreover, with this method, information can be obtained about the mushy region in between, as well as solid and liquid fractions. The application of this method is described on the finless LHTES heated at 50 W from the left as given in Fig. 7. Existing infrared temperature contours were analysed with ThermaCAM Researcher software to obtain a histogram of temperature distribution. The temperature distribution range of the histograms was adjusted to coincide with the onset melting ($T_{om} = 32\ ^{\circ}C$) and endset melting ($T_{em} = 41\ ^{\circ}C$) temperatures obtained from DSC. The temperature histograms prepared for calculation are given in Fig. 7 for 20, 40 and 60 min. At the temperature histogram, the percent summation of temperatures below 32 °C gives the solid fraction, the percent summation of temperatures between 32 and 41 °C gives the mushy zone fraction, and the percent summation of temperatures above 41 °C gives the liquid fraction. For example, the solid, mushy and liquid fractions of the PCM in the LHTES heated from the left at 50 W after 20 min are 61.1%, 13.4% and 25.5%, respectively.

The time-dependent liquid fractions for finless and fins equipped configurations were compared in Fig. 8 at 30 W, 40 W, and 50 W. Despite their poor melting performance at first, finned configurations exhibit enhanced performance after certain breakeven points. The performance enhancements are more pronounced at high heating rates. Moreover, Fin 2 and Fin 3, which are equipped based on melting nature, provide faster liquid formation than Fin 1. As expected, inserting the non-functional fin length on the upper side to the lower region is effective in melting the critical right lower region. It was observed that Fin 3 is effective at high melting rates, while Fin 2 is effective at low

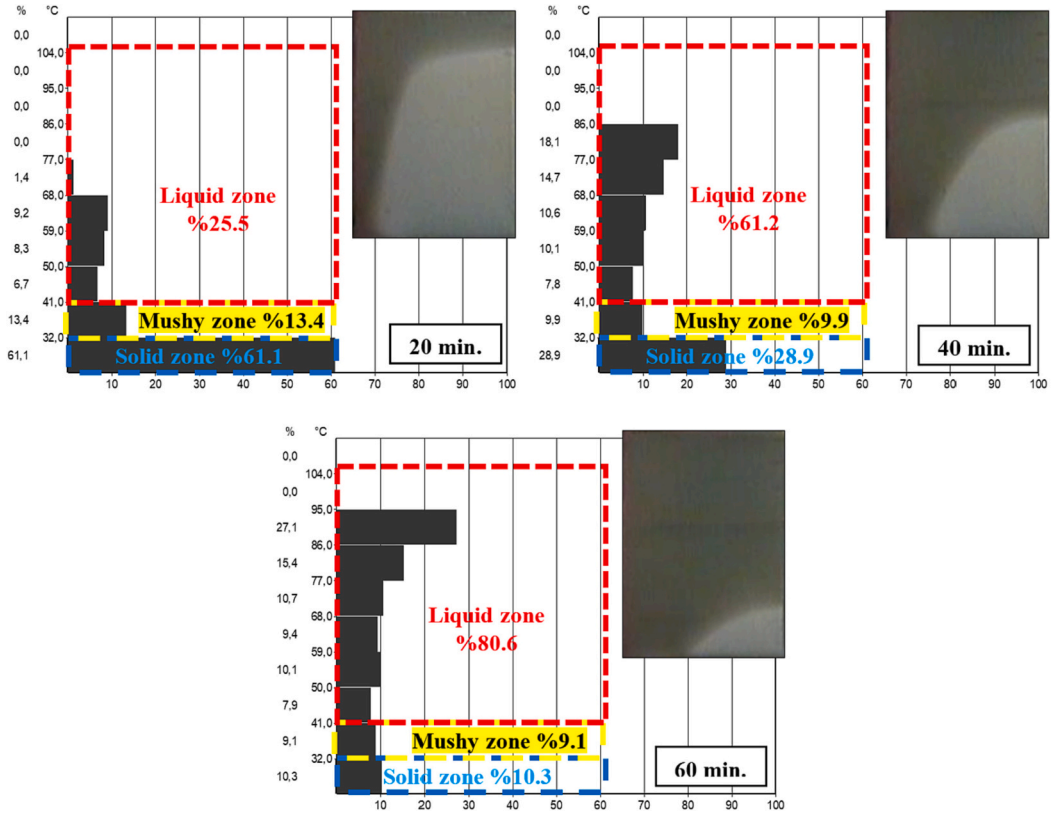

Fig. 7. Temperature histogram bar used in the method of determining mass fraction ratios.

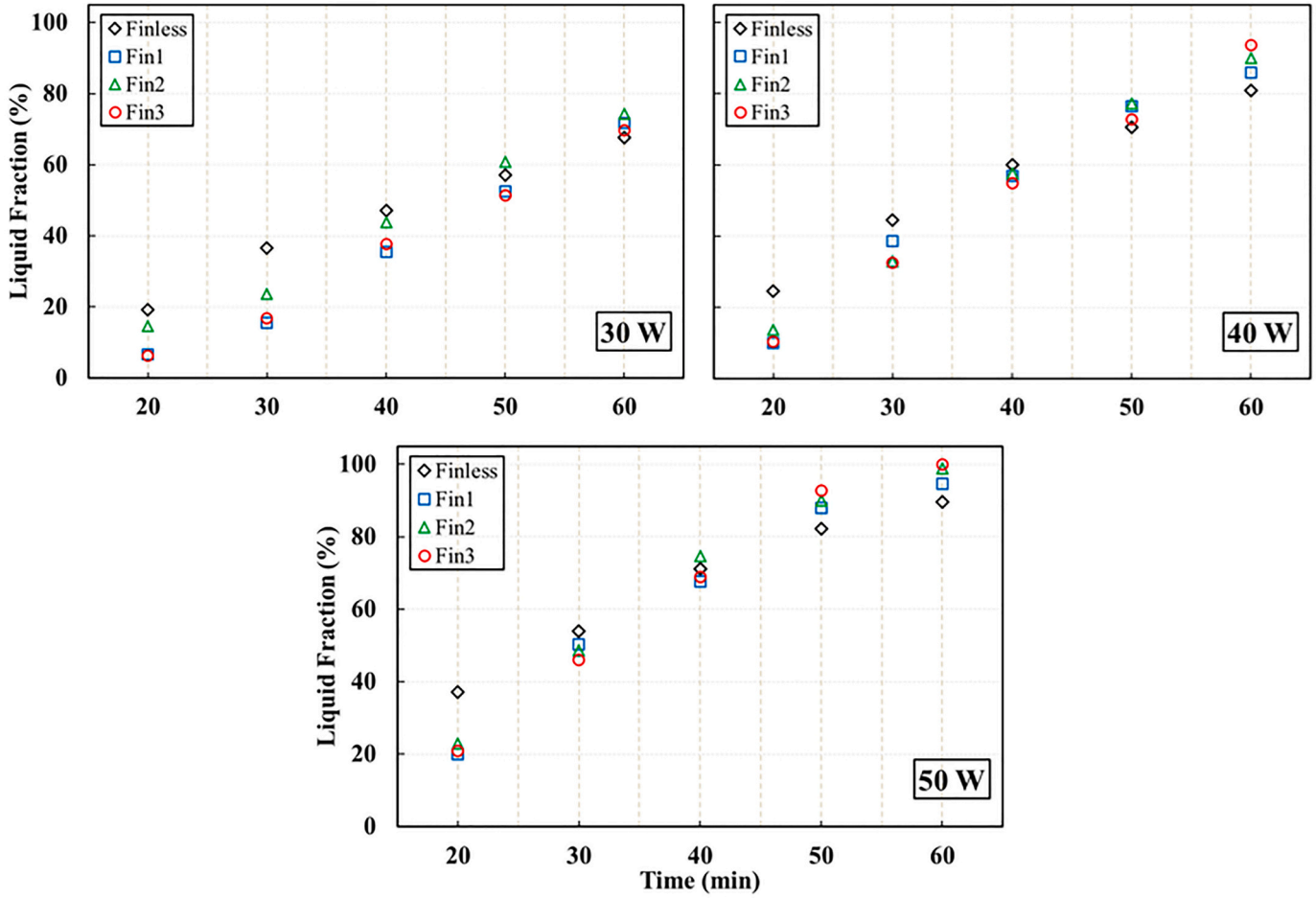

Fig. 8. The time-dependent liquid fractions for different fin arrangements.

melting rates.

The complete melting times of the PCM in the LHTES for 30 W, 40 W and 50 W heating powers were determined using Fig. 9. It was determined as the duration of time when the temperature in the lower right corner of the LHTES (T_3) exceeded the melting endset temperature (T_{me} = 41 °C). As expected, the complete melting time is significantly shortened in finned arrangements for all heating powers. Moreover, Fin 2 and Fin 3 arrangements are also more successful in shortening the melting time compared to Fin 1. For instance, while the melting time of the finless LHTES at 30 W heating power is 6538 s, it is shortened to 5389 s in the LHTES equipped with equal fins, namely Fin 1. Melting times are measured in Fin 2 and Fin 3 arrangements as 4841 and 4913 s, respectively. Similar performance improvements are valid for LHTES heated with 40 W and 50 W power.

Fig. 10 illustrates the comparison of melting time performance enhancements (MTPE) compared to finless LHTES. MTPE values for Fin 1, Fin 2 and Fin 3 at 30 W were calculated to be %17.6, %26 and %24.9, respectively. The MTPE of Fin 1 decreases as the heating power increases, whereas Fin 2 and Fin 3 maintain their MTPE values. For instance, at 50 W heating power, Fin 1's MTPE is 12.8%, whereas the MTPEs of Fin 2 and Fin 3 are 26.3% and 27.7%, respectively. The arrangement of the fin structure in accordance with the nature of the melting (Fin 2 and Fin 3) performs better than Fin 1 in terms of shortening the melting time. Furthermore, the performance enhancements mentioned above increase as the heating power increases. It was observed that although Fin 2 and Fin 3 have similar MTPE performance, Fin 2 performs better at low heating powers while Fin 3 performs better at higher heating powers.

Melting time performance enhancements (MTPE) compared to finless LHTES were calculated with the following equation.

$$MTPE(\%) = \left|\frac{t_{fin} - t_{finless}}{t_{finless}}\right| x100 \quad (3)$$

where t_{fin} and $t_{finless}$ are the total melting times for finned and finless LHTES, respectively.

Fig. 11 shows the variation of LHTES temperature over time for different fins arrangements and for the finless case. The LHTES temperature is the average of the temperatures taken from 9 different points within the LHTES. In order to make an equivalent comparison of the LHTES temperature distribution, the full melting time is dimensionless. The LHTES temperature was significantly reduced compared to the finless case using different fin arrangements. A lower LHTES temperature during complete melting is essentially a measure of more homogenous temperature distribution. The use of fins within the LHTES results in more homogeneous temperature distribution, as shown in Fig. 11. When comparing the finless and Fin 1 arrangements, it can be seen that the LHTES temperature is reduced by around 11 °C for all heating cases. Furthermore, Fin 2 and Fin 3 configurations also provide an extra temperature reduction of around 10 °C over Fin 1. For instance, at 50 W heating, Fin 2 and Fin 3 have lower LHTES temperatures than Fin 1 by 11.7 °C and 9.8 °C, respectively.

4. Conclusions

In this study, the experimental liquid fraction calculation for left-side heated LHTES and the effect of variable fin length arrangements on the melting time were investigated. The results obtained are summarized

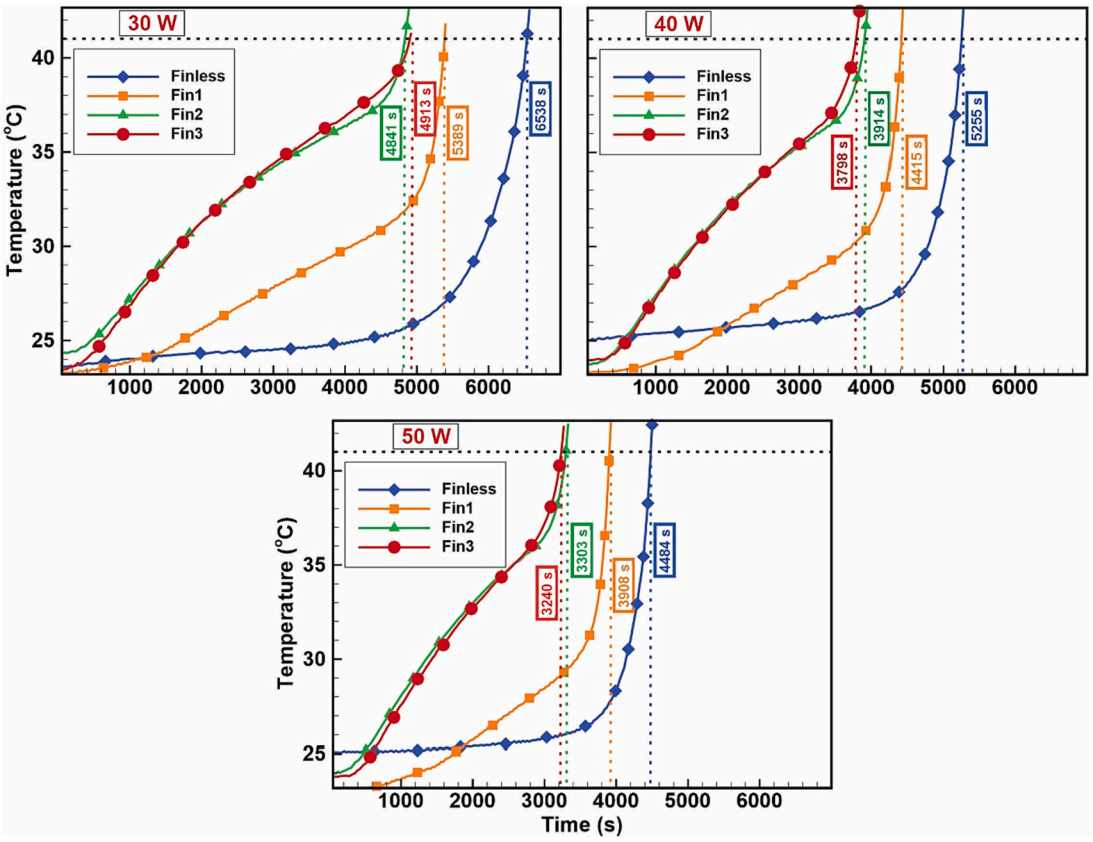

Fig. 9. The complete melting times for LHTES equipped with different fin arrangements.

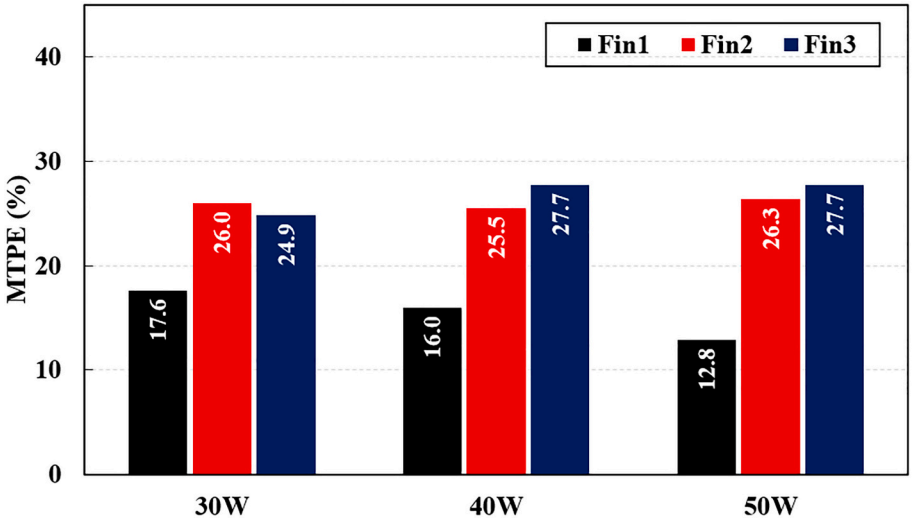

Fig. 10. Melting time performance enhancements (MTPE) compared to finless LHTES.

below.

- It is possible to determine the fractions of solid, mushy, and liquid zones by analysing the temperature histograms of the thermal images of the melting zone.
- Although all fin arrangements negatively affect buoyancy movements during the initial phases of melting, the increased mushy zone contributes to a better melting performance.
- Fin arrangement appropriate for the nature of melting allows buoyancy movements to take place, resulting in better melting performance.
- Compared to finless LHTES, Fin 1 reduces the total melting time by 17.6% to 12.8% depending on the heating rates. However, with the Fin 2 or Fin 3 arrangement, the total melting time is reduced by an extra 8.4% to 14.9% depending on the heating rate.
- Although their melting performances are close to each other, Fin 2 tends to melt better at low heat rates and Fin 3 at high heat rates.

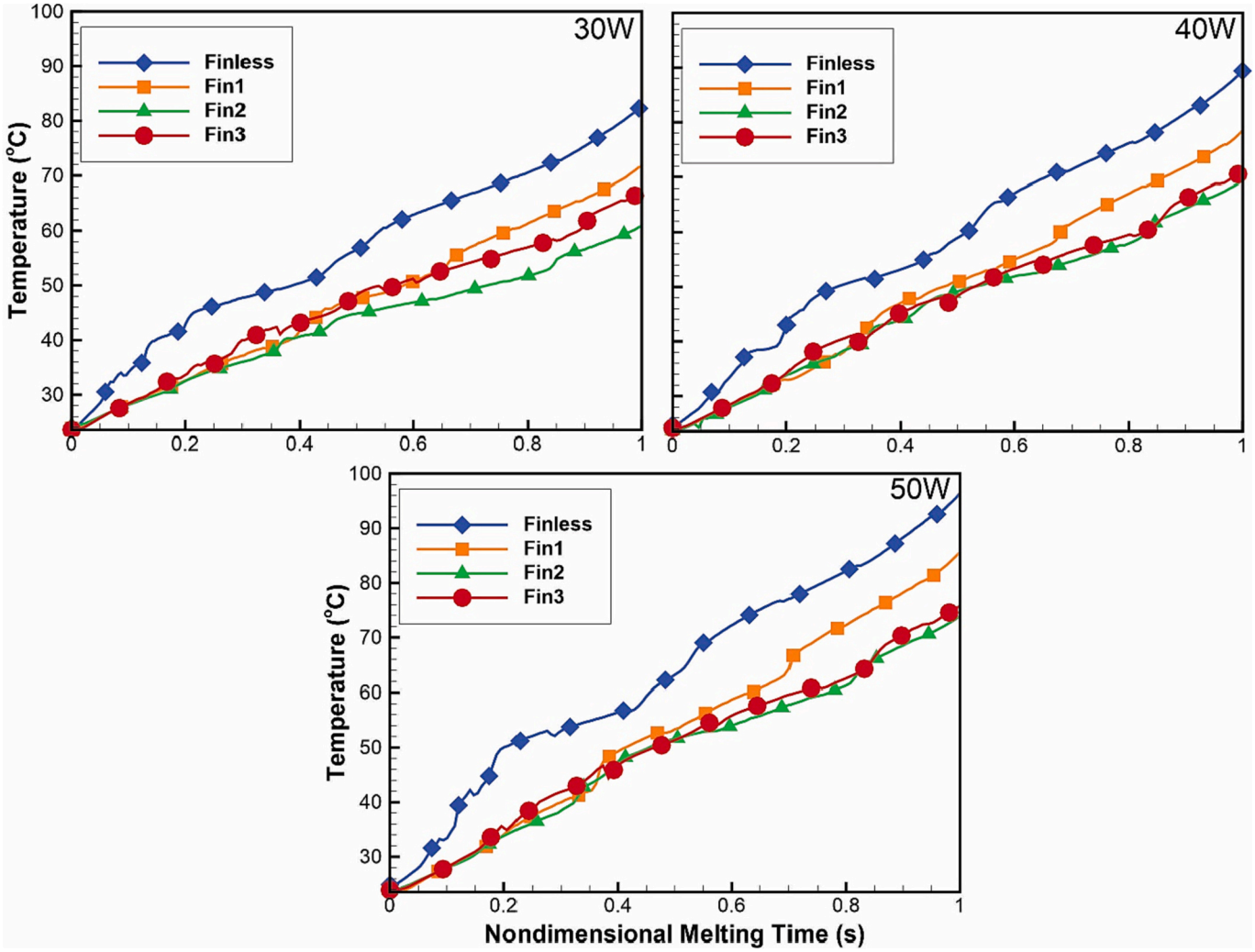

Fig. 11. Variation of LHTES average temperature with respect to nondimensional melting time.

- Compared to finless LHTES, Fin 1 reduces the LHTES average temperature by around 11 °C at all heating rates. However, with the Fin 2 or Fin 3 arrangement, it is reduced by an extra 10 °C depending on the heating rate.
- Using fin arrangements appropriate to the melting process ensures a more uniform melting temperature within the LHTES.

In future work, it is aimed to accelerate the melting even more by using perforated fins arrangements that are appropriate to the nature of the melting.

CRediT authorship contribution statement

Umit Nazli Temel: Investigation, Conceptualization, Methodology, Writing – original draft, Validation, Visualization, Supervision. **Ferhat Kilinc:** Data curation, Methodology, Software, Visualization, Writing – review & editing.

Declaration of Competing Interest

The authors declare that they have no known competing financial interests or personal relationships that could have appeared to influence the work reported in this paper.

Data availability

No data was used for the research described in the article.

References

[1] J. Chen, et al., Effects of different phase change material thermal management strategies on the cooling performance of the power lithium ion batteries: a review, J. Power Sources 442 (September) (2019) 227228, https://doi.org/10.1016/j.jpowsour.2019.227228.
[2] W.L. Cheng, B.J. Mei, Y.N. Liu, Y.H. Huang, X.D. Yuan, A novel household refrigerator with shape-stabilized PCM (phase change material) heat storage condensers: an experimental investigation, Energy 36 (10) (2011) 5797–5804, https://doi.org/10.1016/j.energy.2011.08.050.
[3] S.M. Wang, P. Matiašovský, P. Mihálka, C.M. Lai, Experimental investigation of the daily thermal performance of a mPCM honeycomb wallboard, Energy Build. 159 (2018) 419–425, https://doi.org/10.1016/j.enbuild.2017.10.080.
[4] C. Yao, X. Kong, Y. Li, Y. Du, C. Qi, Numerical and experimental research of cold storage for a novel expanded perlite-based shape-stabilized phase change material wallboard used in building, Energy Convers. Manag. 155 (June 2017) (2018) 20–31, https://doi.org/10.1016/j.enconman.2017.10.052.
[5] X. Cheng, X. Zhai, R. Wang, Thermal performance analysis of a packed bed cold storage unit using composite PCM capsules for high temperature solar cooling application, Appl. Therm. Eng. 100 (2016) 247–255, https://doi.org/10.1016/j.applthermaleng.2016.02.036.
[6] A.E. Kabeel, A. Khalil, S.M. Shalaby, M.E. Zayed, Experimental investigation of thermal performance of flat and v-corrugated plate solar air heaters with and without PCM as thermal energy storage, Energy Convers. Manag. 113 (2016) 264–272, https://doi.org/10.1016/j.enconman.2016.01.068.
[7] M.H. Mahfuz, M.R. Anisur, M.A. Kibria, R. Saidur, I.H.S.C. Metselaar, Performance investigation of thermal energy storage system with phase change material (PCM)

for solar water heating application, Int. Commun. Heat Mass Transf. 57 (2014) 132–139, https://doi.org/10.1016/j.icheatmasstransfer.2014.07.022.
[8] M.T. Johansson, M. Söderström, Electricity generation from low-temperature industrial excess heat-an opportunity for the steel industry, Energy Effic. 7 (2) (2014) 203–215, https://doi.org/10.1007/s12053-013-9218-6.
[9] A. Kaizawa, et al., Thermophysical and heat transfer properties of phase change material candidate for waste heat transportation system, Heat Mass Transf. und Stoffuebertragung 44 (7) (2008) 763–769, https://doi.org/10.1007/s00231-007-0311-2.
[10] C. Muratore, S.M. Aouadi, A.A. Voevodin, Embedded phase change material microinclusions for thermal control of surfaces, Surf. Coat. Technol. 206 (23) (2012) 4828–4832, https://doi.org/10.1016/j.surfcoat.2012.05.030.
[11] D. Mondieig, F. Rajabalee, A. Laprie, H.A.J. Oonk, T. Calvet, M.A. Cuevas-Diarte, Protection of temperature sensitive biomedical products using molecular alloys as phase change material, Transfus. Apher. Sci. 28 (2) (2003) 143–148, https://doi.org/10.1016/S1473-0502(03)00016-8.
[12] H. Ohkawara, T. Kitagawa, N. Fukushima, T. Ito, Y. Sawa, T. Yoshimine, A newly developed container for safe, easy, and cost-effective overnight transportation of tissues and organs by electrically keeping tissue or organ temperature at 3 to 6°C, Transplant. Proc. 44 (4) (2012) 855–858, https://doi.org/10.1016/j.transproceed.2012.02.023.
[13] W.Q. Li, Z.G. Qu, Y.L. He, Y.B. Tao, Experimental study of a passive thermal management system for high-powered lithium ion batteries using porous metal foam saturated with phase change materials, J. Power Sources (2014), https://doi.org/10.1016/j.jpowsour.2014.01.006.
[14] Z. Rao, Y. Huo, X. Liu, G. Zhang, Experimental investigation of battery thermal management system for electric vehicle based on paraffin/copper foam, J. Energy Inst. 88 (3) (2015) 241–246, https://doi.org/10.1016/j.joei.2014.09.006.
[15] D. Zou, X. Ma, X. Liu, P. Zheng, Y. Hu, Thermal performance enhancement of composite phase change materials (PCM) using graphene and carbon nanotubes as additives for the potential application in lithium-ion power battery, Int. J. Heat Mass Transf. 120 (2018) 33–41, https://doi.org/10.1016/j.ijheatmasstransfer.2017.12.024.
[16] F. Bahiraei, A. Fartaj, G.A. Nazri, Experimental and numerical investigation on the performance of carbon-based nanoenhanced phase change materials for thermal management applications, Energy Convers. Manag. (2017), https://doi.org/10.1016/j.enconman.2017.09.065.
[17] S.F. Hosseinizadeh, F.L. Tan, S.M. Moosania, Experimental and numerical studies on performance of PCM-based heat sink with different con fi gurations of internal fi ns q, Appl. Therm. Eng. 31 (17–18) (2011) 3827–3838, https://doi.org/10.1016/j.applthermaleng.2011.07.031.
[18] A. Abdi, V. Martin, J.N.W. Chiu, Numerical investigation of melting in a cavity with vertically oriented fins, Appl. Energy 235 (November 2018) (2019) 1027–1040, https://doi.org/10.1016/j.apenergy.2018.11.025.
[19] A. Acır, M. Emin Canlı, Investigation of fin application effects on melting time in a latent thermal energy storage system with phase change material (PCM), Appl. Therm. Eng. 144 (September) (2018) 1071–1080, https://doi.org/10.1016/j.applthermaleng.2018.09.013.
[20] M.J. Huang, P.C. Eames, B. Norton, N.J. Hewitt, Solar energy materials & solar cells natural convection in an internally finned phase change material heat sink for the thermal management of photovoltaics, Sol. Energy Mater. Sol. Cells 95 (7) (2011) 1598–1603, https://doi.org/10.1016/j.solmat.2011.01.008.
[21] M.H. Joneidi, M. Rahimi, R. Pakrouh, R. Bahrampoury, Experimental analysis of transient melting process in a horizontal cavity with different con fi gurations of fi ns, Renew. Energy 145 (2020) 2451–2462, https://doi.org/10.1016/j.renene.2019.07.114.
[22] B. Kamkari, H. Shokouhmand, International journal of heat and mass transfer experimental investigation of phase change material melting in rectangular enclosures with horizontal partial fins, Int. J. Heat Mass Transf. 78 (2014) 839–851, https://doi.org/10.1016/j.ijheatmasstransfer.2014.07.056.
[23] L.L. Tian, X. Liu, S. Chen, Z.G. Shen, Effect of fin material on PCM melting in a rectangular enclosure, Appl. Therm. Eng. 167 (April) (2019) 2020, https://doi.org/10.1016/j.applthermaleng.2019.114764.
[24] P.H. Biwole, D. Groulx, F. Souayfane, T. Chiu, Influence of fin size and distribution on solid-liquid phase change in a rectangular enclosure, Int. J. Therm. Sci. 124 (April 2017) (2018) 433–446, https://doi.org/10.1016/j.ijthermalsci.2017.10.038.
[25] C. Ji, Z. Qin, Z. Low, S. Dubey, F.H. Choo, F. Duan, Non-uniform heat transfer suppression to enhance PCM melting by angled fins, Appl. Therm. Eng. 129 (2018) 269–279, https://doi.org/10.1016/j.applthermaleng.2017.10.030.
[26] C. Ji, Z. Qin, S. Dubey, F.H. Choo, F. Duan, Simulation on PCM melting enhancement with double-fin length arrangements in a rectangular enclosure induced by natural convection, Int. J. Heat Mass Transf. 127 (2018) 255–265, https://doi.org/10.1016/j.ijheatmasstransfer.2018.07.118.
[27] S. Zhang, L. Pu, S. Mancin, M. Dai, L. Xu, Role of partial and gradient filling strategies of copper foam on latent thermal energy storage: an experimental study, Energy 255 (2022), 124517, https://doi.org/10.1016/j.energy.2022.124517.
[28] A.I.N. Korti, H. Guellil, Experimental study of the effect of inclination angle on the paraffin melting process in a square cavity, J. Energy Storage 32 (April) (2020) 1–12, https://doi.org/10.1016/j.est.2020.101726.
[29] M. Fadl, P.C. Eames, An experimental investigations of the melting of RT44HC inside a horizontal rectangular test cell subject to uniform wall heat flux, Int. J. Heat Mass Transf. 140 (2019) 731–742, https://doi.org/10.1016/j.ijheatmasstransfer.2019.06.047.
[30] T. Okabe, T. Miyanishi, T. Miyagawa, H. Murata, Spatio-temporal measurement of natural convective heat transfer on melting process using infrared thermography, Int. J. Heat Mass Transf. 181 (2021), 121882, https://doi.org/10.1016/j.ijheatmasstransfer.2021.121882.
[31] J.P. Holman, Experimental Methods for Engineers, 7th ed., McGraw-Hill, New York, 2011.